# Recent Advances in 0D Ni/Co-based Hollow Electrocatalysts for Electrochemical Water Splitting

GE Wenjing, CHEN Xiaocui, MA Ruizhao, ZHENG Siyuan, SHANG Ningzhao and ZHAO Xiaoxian✉

Electrochemical water splitting using renewable energy sources has been recognized as a sustainable way to produce hydrogen energy due to the characteristics of low-carbon and no pollution. However, the slow hydrogen/oxygen evolution reactions (HER/OER) seriously hinder the practical application of large-scale water splitting. In this paper, the 0D Ni/Co-based hollow material is discussed in detail because of adjustable morphology, low mass density and abundant active sites, which provides an effective solution for improving the HER/OER reaction kinetics. The synthesis methods of hollow materials, such as hard template, soft template and self-template are introduced. Afterward, catalysts with different structural designs of hollow structures are reviewed, including hollow single-shelled structure, hollow core-shelled structure, hollow double-shelled structure and hollow multi-shelled structure (HoMS) catalysts. Wherein, the research progress of the 0D Ni/Co-based HoMS electrocatalysts in recent years and their prominent performances in water splitting are highlighted. Finally, the challenges and development prospects of designing Ni/Co-based HoMS catalysts in water splitting in the future are discussed.
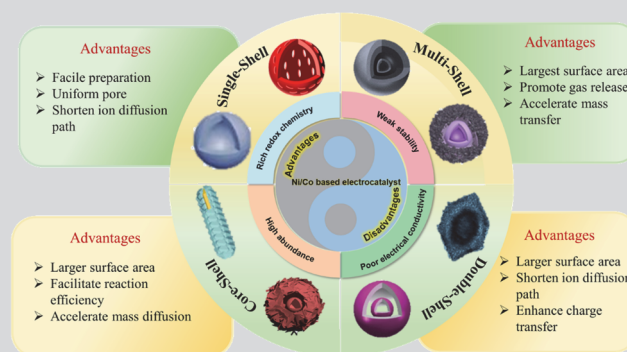
1 Introduction

With the large-scale consumption of traditional fossil fuels and global warming caused by climate change, energy crisis and environmental pollution make people urgently pursue clean, efficient and sustainable energy.[1−5] Hydrogen has been considered as an ideal and the cleanest fuel, which has high energy density, superior calorific value (142351 kJ/kg) and no pollution characteristics.[6−8] Electrochemical water splitting is a green approach to producing green hydrogen,[9−11] which consists of two reactions, one is oxygen evolution reaction (OER) of the anode, and another is hydrogen evolution reaction (HER) of the cathode.[12−16] Currently, noble metal-based catalysts (Pt for HER and IrO_2 or RuO_2 for OER) are still state-of-the-art electrocatalyst candidates for hydrogen production with excellent electrochemical activity.[17−19] However, noble metal-based catalysts of scarcity, high cost and low stability have severely hindered their widespread applications.[20−22] Enormous efforts have been made to investigate non-noble metal-based electrocatalysts with low cost, remarkable activity and distinguished durability for water splitting.

The transition metal compounds, such as metal oxides,[11,23−26] hydroxides,[27−29] sulfides,[30−32] phosphates,[33−35] nitrides,[36−38] or alloys[39−41] with abundant resource are adapted to improve the activity of electrocatalysts. Among them, Ni/Co-based compounds have received much attention in water splitting as promising electrocatalysts due to their rich redox chemistry, high abundance, relatively low cost, and moderate ability to absorb and desorb intermediates.[42] Nevertheless, the poor electrical conductivity and reduction of active sites caused *via* nanoparticle agglomeration have hindered their wide application in electrocatalysis.[43]

As shown in Fig. 1, there are two aspects to increase electrocatalytic activity, one is to augment a mass of active sites, and the other is to enhance the inherent activity of the catalyst.[44] Morphological regulation is an effective strategy to promote the exposure of active sites for enhancing the activity of electrocatalysis. Particularly, the hollow nano catalysts have captured extensive attention for boosting OER/HER because of the combination of structural regulation and compositional engineering advantages. On one hand, the hollow structures possess adjustable

✉ ZHAO Xiaoxian
lxzhxx@hebau.edu.cn
Department of Chemistry, College of Science, Hebei Agricultural University, Baoding 071001, P. R. China
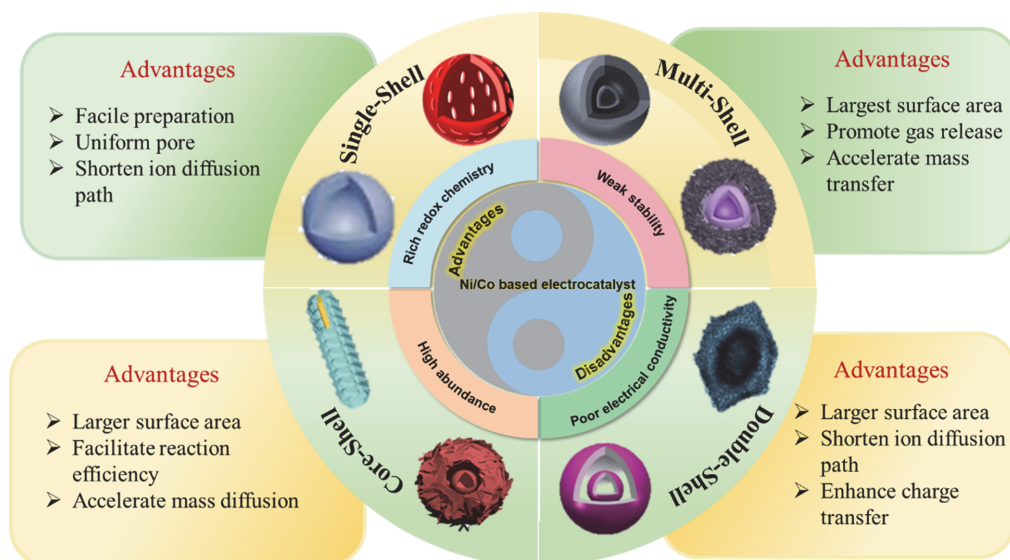
Fig. 1 Schematic of morphology design strategy of 0D Ni/Co-based hollow material for high-performance water splitting

morphology with a large number of pores, thus to increasing the contact area between electrolyte and electrode, providing numerous active surface areas.[26,45−48] On the other hand, large void space and thin shell can shorten the ion transport and charge transfer pathways, improving the reaction kinetics.[49−52] Designing 0D Ni/Co-based hollow material must improve the electrocatalytic activity and stability for water splitting.

The 0D Ni/Co-based hollow material can be devided into four kinds: hollow single-shelled structure, hollow core-shelled structure, hollow double-shelled structure and hollow multi-shelled structure (HoMS) as shown in Fig. 1. Generally, the synthesis methods of hollow electrocatalysts include hard template,[53,54] soft template[55] and self-supported template.[56−58] In this paper, the application of 0D Ni/Co-based hollow electrocatalysts in water splitting in recent years is reviewed, and based on the different synthesis approaches we discuss the characteristics of different structures. Each structure exhibits its own characteristics to conquer the disadvantages of nano electrocatalysts. To be specific, the hollow single-shelled structure has a relatively simple preparation process, uniform pore, to shorten the path of ion diffusion, which improves electrocatalytic activity. Meanwhile, hollow single-shelled structure materials are easy to cause the aggregation of active species. Compared with hollow single-shelled structure, hollow core-shelled structure provides a larger surface area, facilitates reaction efficiency, and accelerates mass diffusion, which is conducive to further improving the electrocatalyst activity and stability. For hollow double-shelled structure materials, there is a large gap between the shells, increasing specific surface area, enhancing charge transfer, and

shortening ion diffusion path. Compared with the above hollow structures, HoMS has the largest surface area, promotes gas release, and accelerates mass transfer because of the better utilization of internal space, which exhibits outstanding activity and good stability. All in all, with the transformation of structure from single-shelled to multi-shelled, the relative contacting area between hollow particles is decreased due to the increased high utilization of internal volume for more active sites. Hollow structure electrocatalyst exhibits outstanding OER/HER activity and stability due to their optimized electronic structure, good conductivity and abundant active surface area, especially the Ni/Co-based HoMS electrocatalyst due to its unique structure for more active sites. Finally, we briefly discuss the challenges and directions of designing Ni/Co-based HoMS catalysts for water splitting in the future.

2 Ni/Co-based Hollow Materials

### 2.1 Ni/Co-based Hollow Single-shelled Structure

Hollow single-shelled structure has attracted numerous research attention owing to adjustable morphology, which leads to superior durable stability. In addition, the porous hollow structure materials have uniform pore size distribution to facilitate the permeation of electrolytes and shorten the ion diffusion path, which is beneficial to increase more active sites to enhance the electrochemical performances.[59−61] For example, Xia and co-workers[62] have synthesized hollow single-shelled and porous heterostructure $Co_3O_4/CoMoO_4$ hybrids using carbon spheres as templates by hard template-assisted strategy

(Fig. 2A). The scanning electron microscopy (SEM) and transmission electron microscopy (TEM) images show that the surface of carbon spheres becomes rough after adsorbing metal ions and high-temperature carbonization process (Fig. 3, A and B). Especially, the $Co_3O_4/CoMoO_4$-0.1-FO catalyst delivers smaller Tafel (72 mV/dec) in 1.0 mol/L KOH, which is much lower than that of the commercial RuO_2, implying a faster reaction kinetics (Fig. 4A). As shown in the Nyquist plots (Fig. 4B), the $Co_3O_4/CoMoO_4$-0.1-FO catalyst shows a lower charge transfer resistance than other samples, indicating hollow porous structure can accelerate the reaction kinetics and improve electrocatalytic activity. It is believed that the porous structure is conducive to mass diffusion and charge transfer, which further enhances the electrocatalytic activity of the catalyst. Generally speaking, the advantage of the hard template is that it can be used to exactly adjust the size, structure and morphology, which has got much attention. Li and co-workers[63] have developed hollow single-shelled CoFe/N-HCSs by using the PS microspheres prepared *via* chemical oxidation polymerization as hard templates through the chelation of Co^{2+} and Fe^{2+} ions with ligand and finally pyrolysis at high temperature (Fig. 2B). The SEM image shows that the CoFe/N-HCSs have the same uniform spherical structure as the precursor. The TEM image further shows that the morphology of the catalyst CoFe/N-HCSs is that the CoFe-ZIF particles are uniformly attached to the hollow sphere because the chelation effect of the amino (—NH—) groups in PPy chains with metal ion can efficiently avoid the agglomeration of CoFe-ZIF crystals (Fig. 3, C and D). Owing to the coupling between the highly conductive N-HCSs support and remarkable activity CoFe-ZIF, the hollow single-shelled CoFe/N-HCSs could have smaller Tafel (58 mV/dec) in alkaline electrolyte, which displays superior OER performance (Fig. 4C). Moreover, the calculated double-layer capacitance (C_{dl}) of CoFe/N-HCSs is 37.1 mF/cm^2, outperforming than that of other corresponding materials owing to unique hollow structure with abundant active sites and large surface area (Fig. 4D).[63]

The approaches to synthesizing hollow single-shelled structures include not only hard templates, but also soft templates and self-supported templates. Guo and co-workers[64] have reported a soft template method to synthesize hollow H-Fe-CoMoS heterostructures. Compared with the hard template, the soft template is more flexible and adjustable, because the soft template is mainly amphiphilic molecules that can form an ordered aggregate, so it is relatively easy to remove. The surfactant in the soft template can form micelles in the solution, thus guiding the growth of the precursor, and finally generating a nanostructured material with a certain shape. The hollow single-shelled H-Fe-CoMoS heterostructures (H-Fe-CoMoS) were obtained by

self-assembly into micelles using triblock copolymers as soft templates. And after the calcination process, the micelles of the soft template were removed and the hollow H-Fe-CoMoS heterostructures were obtained (Fig. 2C). The SEM image and the TEM images show the formation of hollow spherical particles. The TEM images further demonstrate that these hollow spheres thickness is about 10 nm and the diameters of the voids corresponded roughly to those of PS-b-PAA-b-PEG micelles (Fig. 3, E and F). The H-Fe-CoMoS has lower overpotential and smaller Tafel (58 mV/dec) for OER and smaller Tafel (98 mV/dec) for HER in 1.0 mol/L KOH, demonstrating that the construction of hollow structures and the addition of Fe doping significantly boost the catalytic activity of H-Fe-CoMoS in the water splitting (Fig. 4, E and F). Compared to the hard/soft templates, self-templated strategies have attracted more and more attention, which can directly convert reactants into hollow structure without extra templates removal process. Recently, due to the adjustable structure and composition, metal-organic frameworks (MOF) have been regarded as ideal self-templates for hollow structure catalysts.[65] As shown in Fig. 2D, Feng *et al.*[66] have reported that ZIF-67 nano-cubes (ZIF-67 NCs) firstly were synthesized and etched by tannic acid to form hollow ZIF-67 nano-cubes (HZIF-67 NCs), and then calcined with Cu foam under nitrogen atmosphere to prepare hollow single-shelled CoCu@HNC electrocatalysts. The SEM image shows that ZIF-67 NCs, HZIF-67NCs and CoCu@HNC have a similar uniform cubic morphology while CoCu@HNC surfaces become rough. The TEM image further demonstrates that the CoCu@HNC morphology of a hollow cube structure is formed with a shell thickness of 26 nm (Fig. 3, G and H). CoCu@HNC shows the best electrocatalytic performance both for HER and OER in 1.0 mol/L KOH compared to those of counterparts. The Tafel slope of CoCu@HNC (88.6 mV/dec) is lower than that of RuO_2 (102.4 mV/dec), suggesting the outstanding OER activity and faster reaction dynamics. The hollow single-shelled CoCu@HNC catalyst also shows the best HER performance with a low Tafel slope of 30.62 mV/dec, surpassing those of counterparts (Fig. 4, G and H).

Based on morphology regulation, heteroatom doping has been shown to be effective in regulating the electron structure and increasing the number of catalytic active sites to enhance electrocatalytic activity. Guo *et al.*[67] have reported a facile ion-assisted etching method employing ZIF-8 rhombic dodecahedron as the template to obtain hollow single-shelled Ir-Ni(OH)$_2$ nanocage (Fig. 2E). In this work, heteroatom doping is mainly carried out by a simple ion-exchange method. The TEM images clearly indicate that hollow nanocages were successfully prepared (Fig. 3, I and J). The highly open nanocage structure and the large void not only enable the catalyst to expose more surface of active sites,
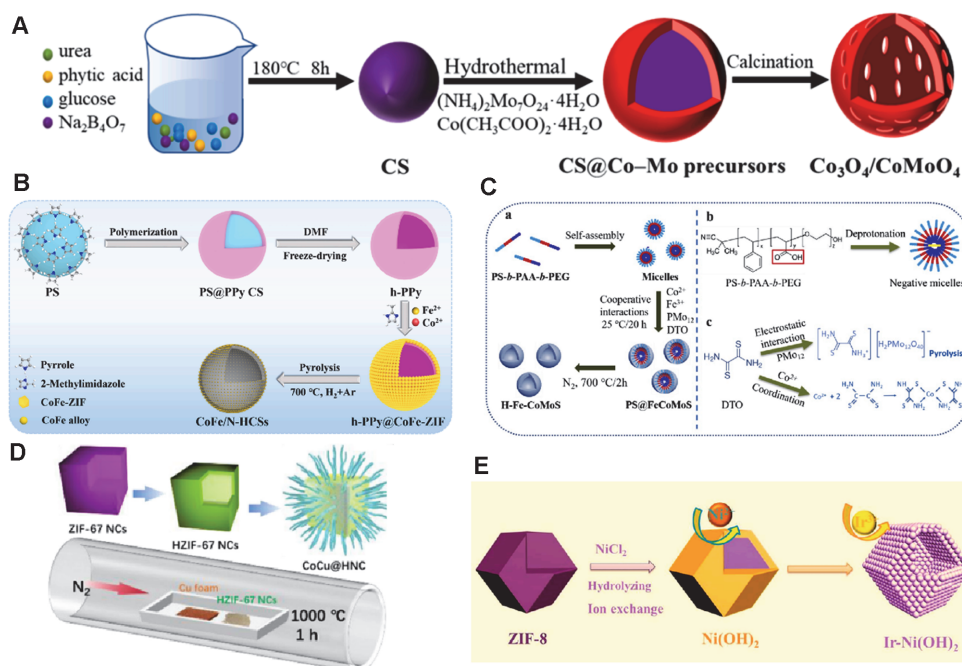
Fig. 2 Schematic illustration for the preparation of hollow single-shelled Co₃O₄/CoMoO₄ (A), diagram of the synthesis process of hollow single-shelled CoFe/N-HCSs (B), schematic illustration of preparation for hollow single-shelled H-Fe-CoMoS (C), schematically presenting the synthesis of hollow single-shelled CoCu@HNC catalyst (D) and schematic illustration for the preparation of hollow single-shelled Ir-Ni(OH)₂ nanocages (E)

(A) Reprinted with permission from ref. [62], Copyright 2023, Elsevier; (B) reprinted with permission from ref. [63], Copyright 2021, Elsevier; (C) reprinted with permission from ref. [64], Copyright 2020, Elsevier; (D) reprinted with permission from ref. [66], Copyright 2023, Chinese Chemical Society; (E) reprinted with permission from ref. [67], Copyright 2022, Elsevier.
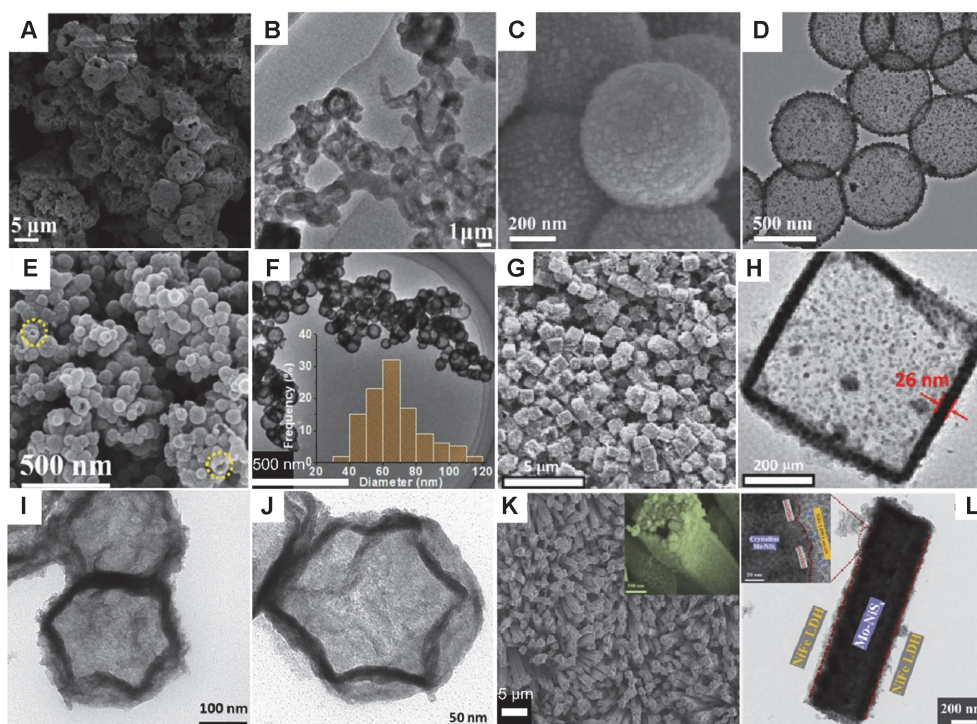
Fig. 3 SEM image and TEM image of hollow single-shelled Co₃O₄/CoMoO₄ (A, B), SEM and TEM images of hollow single-shelled CoFe/N-HCSs (C, D), SEM image and TEM image of hollow single-shelled H-Fe-CoMoS (E, F), SEM image and TEM image of hollow single-shelled CoCu@HNC (G, H), TEM images of hollow single-shelled Ir-Ni(OH)₂ nanocages catalyst (I, J) and SEM image and TEM image of hollow core-shelled Mo-NiSₓ@NiFe LDH/NF (K, L)

(A, B) Reprinted with permission from ref. [62], Copyright 2023, Elsevier; (C, D) reprinted with permission from ref. [63], Copyright 2021, Elsevier; (E, F) reprinted with permission from ref. [64], Copyright 2020, Elsevier; (G, H) reprinted with permission from ref. [66], Copyright 2023, Chinese Chemical Society; (I, J) reprinted with permission from ref. [67], Copyright 2022, Elsevier. (K, L) reprinted with permission from ref. [68], Copyright 2022, The Royal Society of Chemistry.
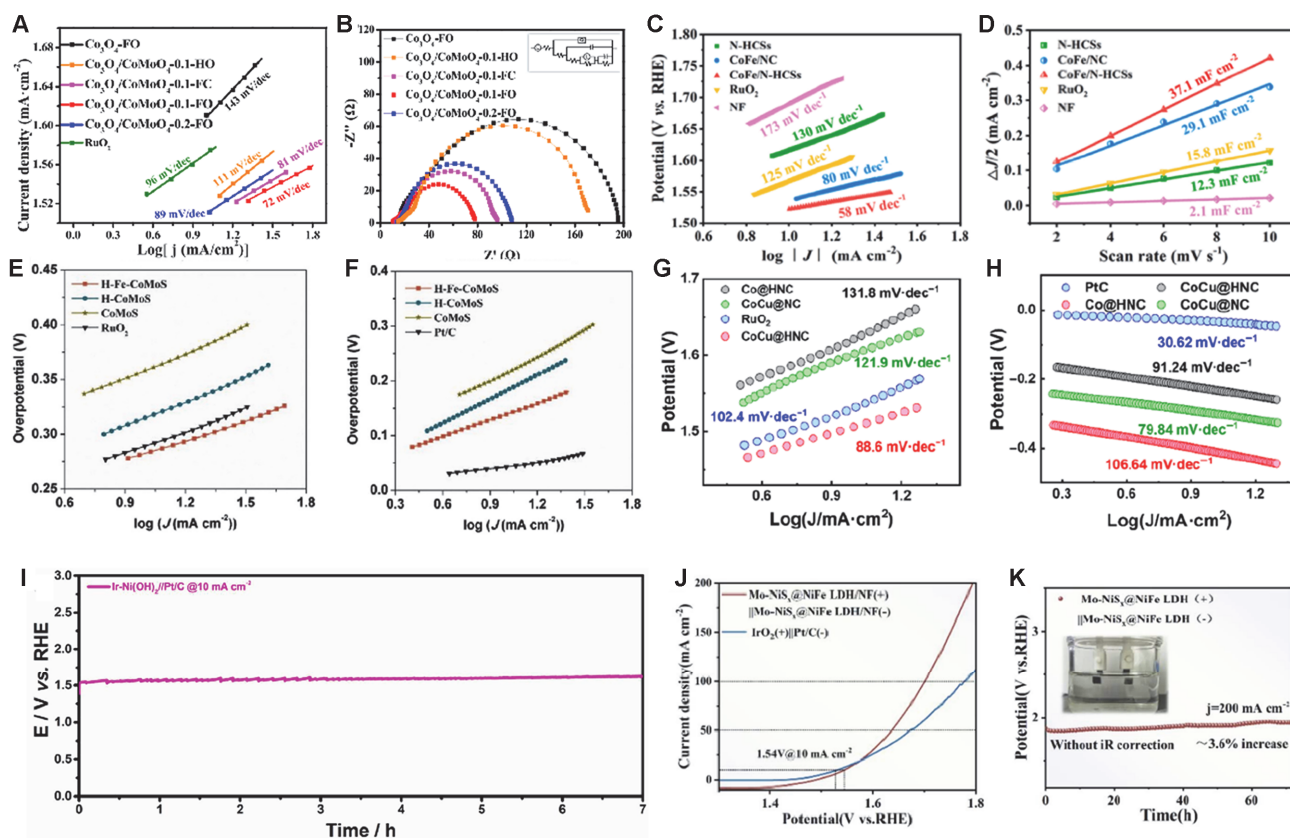
Fig. 4 Tafel plots of porous hollow single-shelled Co₃O₄/CoMoO₄ catalyst and other catalysts (A), Nyquist plots of overpotential (B), Tafel plots of hollow single-shelled CoFe/N-HCSs and other materials for OER (C), plots of current density *versus* the scan rate at 1.24 V (*vs*. RHE) (D), Tafel plots of hollow single-shelled H-Fe-CoMoS and other catalysts for OER in 1.0 mol/L KOH (E), corresponding Tafel plots for HER (F), Tafel plots of hollow single-shelled CoCu@HNC and other samples for OER in 1.0 mol/L KOH (G), corresponding Tafel plots for HER (H), CP curve of the hollow single-shelled Ir-Ni(OH)₂//Pt/C couple for water splitting at the current density of 10 mA/cm² (I), LSV curves of hollow core-shelled Mo-NiSₓ@NiFe LDH/NF electrode (J) and chronopotentiometry measurements for Mo-NiSₓ@NiFe LDH/NF electrode (K)

(A, B) Reprinted with permission from ref. [62], Copyright 2023, Elsevier; (C, D) reprinted with permission from ref. [63], Copyright 2021, Elsevier; (E, F) reprinted with permission from ref. [64], Copyright 2020, Elsevier; (G, H) reprinted with permission from ref. [66], Copyright 2023, Chinese Chemical Society; (I) reprinted with permission from ref. [67], Copyright 2022, Elsevier; (J, K) reprinted with permission from ref. [68], Copyright 2022, The Royal Society of Chemistry.

but also facilitate the mass transport and charge transfer. In addition, electrochemical measurements demonstrate that Ir doping Ni(OH)₂ nanocage with effective surface area exposure as well as the electronic structure modulation exhibits excellent OER activity and durable stability. The two-electrode system composed of Ir-Ni(OH)₂ as anode and Pt/C as cathode [Ir-Ni(OH)₂//Pt/C] can deliver a voltage of 1.55 V and maintain 7 h at the current density of 10 mA/cm², which further indicates Ir-Ni(OH)₂ catalyst has great potential in water splitting (Fig. 4I).

2.2 Ni/Co-based Hollow Core-shelled Structural Materials

Among the strategies of morphology and structure regulation, hollow core-shelled structure has attracted much

attention due to its ability to improve the exposure of active sites and further enhance the electrocatalytic activity. Compared to the hollow single-shelled structure, not only the outer shell can contact with electrolyte, which is similar to the hollow single-shelled structure, but the inner core coated by the shell to avoid active site loss can provide more contact sites with electrolyte. Therefore, the hollow core-shelled structure demonstrates the larger specific surface area to provide a more electrocatalytic active site. Besides, the inner core can support the outer shell to restrain the collapse of the outer shell, which improves the structure stability during cycling. The porous trait of hollow core-shelled structure facilitates the permeation of electrolyte, combing with thin shell and core to decrease transport distance between ions and substances to further improve the electrocatalytic activity.[69—71]

Song and co-worker[68] have synthesized a core-shelled

structure Mo-doped NiS_x nanoarrays (Mo-NiS_x@NiFe LDH/NF) that can enhance the electrocatalytic performance remarkably (Fig. 5A). The hollow core-shelled Mo-NiS_x@NiFe LDH/NF structure was prepared by a hydrothermal method following a vulcanization and electrodeposition approach. The SEM and TEM images show that Mo-NiS_x@NiFe LDH/NF has a core-shelled structure with ultrathin NiFe LDH nanosheets wrapped on microrods of Mo-NiS_x/NF (Fig. 3, K and L). The hollow core-shelled Mo-NiS_x@NiFe LDH/NF can increase active sites and enhance mass transfer, leading to the improved electrocatalytic activity, which is beneficial to the application of water splitting. Therefore the two-electrode system composed of the Mo-NiS_x@NiFe LDH/NF catalyst can be driven only 1.54 V at the current density of 10 mA/cm² in 1 mol/L KOH, and no increase in potential after remaining 60 h at the current density of 200 mA/cm², which is conducive to the application of electrochemical water splitting (Fig. 4, J and K).

Prussian-blue-analogues (PBAs) with the formula $MII_3[MIII(CN)_6]_2$ (M =Fe, Co, Ni, etc.) are a class of MOFs with transition-metal ions bridged by cyano ligand. It is a desirable self-template for constructing hollow core-shelled structures owing to their uniform size, high porosity and adjustable morphology, as well as variable composition.[72−74] Fang and co-workers[75] have developed hollow core-shelled PBA-Se-350 nanocages that were obtained by using FeMn@CoNi core-shelled PBAs as template, following reaction with Se powders in low-temperature pyrolysis under argon (Ar) atmosphere (Fig. 5B). SEM and TEM images show the samples' cubic shape and the uniform distribution of small nanocage particles (Fig. 6, A and B). The regulation of the structure and composition of the hollow nanocages lead to the formation of a highly active species and a larger specific surface. Therefore, the PBA-Se-350 catalyst exhibits an ultralow overpotential and a smaller Tafel slope (43.4 mV/dec), indicating the most outstanding activity for OER and enhancing the mass diffusion (Fig. 7A). In addition, the hollow nanocage PBA-Se-350 displays robust long-term stability at a current density of 100 mA/cm² for 30 h (Fig. 7B). The porous hollow core-shelled structure can facilitate the rapid entry of the electrolyte into the inner cavity and promote the rapid diffusion of the gas in the electrochemical reactions, thus contributing to the improvement of performance and good stability. Hou et al.[76] have prepared a green, safe, and low-cost CoNi nano-alloys modified hollow core-shelled carbon cage (CoNi/NC-YS) catalyst by using saccharomycete to adsorb nickel and cobalt ions after high-temperature pyrolysis process (Fig. 5C). There are rich functional groups on the surface of saccharomycetes, which is conducive to the adsorption of metal ions. The SEM image displays that the

morphology of the CoNi/NC-YS catalyst contains an outer shell composed of a large number of CoNi nano-alloy particles and a carbon core. The TEM image further proves that the CoNi/NC-YS catalyst is a hollow core-shelled structure (Fig. 6, C and D). Benefitting from the unique hollow core-shelled structure, the C_{dl} of the CoNi/NC-YS catalyst (24.63 mF/cm²) is superior to those of corresponding catalysts, indicating that the structure has more active sites (Fig. 7C). Furthermore, due to the strong structure stability of the hollow core-shelled structure, the CoNi/NC-YS catalyst can maintain 24 h stability at a current density of 10 mA/cm² without little attenuation, illustrating outstanding durability in the OER process (Fig. 7D).

Besides the PBAs, other MOFs have been extensively studied in core-shelled structure design owing to their high porosity, larger specific surface area, and adjustable structure.[77] The hollow core-shelled catalyst prepared by constructing a metal-organometallic framework as precursor has both the excellent OER reaction and outstanding HER reaction, which is beneficial for the large-scale application of water splitting. Lou et al.[78] have designed a kind of hollow core-shelled NiCoFe-HO@NiCo-LDH microrods via MOF as self-template following an ion-exchange reaction process (Fig. 5D). Because of mild reaction conditions during the ion-exchange process, the rod-like structures MIL-88A and ZIF-67 are retained, and a hollow core-shelled rod-like morphology of Ni-Co-Fe LDH with the complex surface is achieved. The field emission scanning electron microscope (FESEM) and TEM images show that the nanocages are stably supported on the solid microrod with a hollow space (Fig. 6, E and F). The catalytic activities of the prepared hollow core-shelled NiCoFe-HO@NiCo-LDH YSMRs materials are evaluated by electrochemical test. A remarkable OER activity and a small Tafel slope of 49.7 mV/dec are obtained benefitting from unique structure and compositional virtue (Fig. 7, E and F). Some metal/organic chelates can also be self-template to prepare the hollow core-shelled structure. Kaneti et al.[79] have prepared hierarchical Mn-Co phosphide hollow core-shelled spheres via cobalt glycerate spheres as self-template following a phosphating process (Fig. 5E). As shown in the TEM image and HAADF-TEM image (Fig. 6, G and H), a hollow hierarchical core-shelled nature assembled by 2D nanoplates of Mn-Co-P is detected. Compared with other samples, some small nanoparticles on the surface of nanoplate are observed attributed to the phosphating process. The hollow hierarchical core-shelled sphere Mn-Co-P delivers high OER activity with a lower overpotential (330 mV) and a smaller Tafel slope (59 mV/dec) at a current density of 10 mA/cm², which is outperforming than those of catalysts (Fig. 7, G and H).
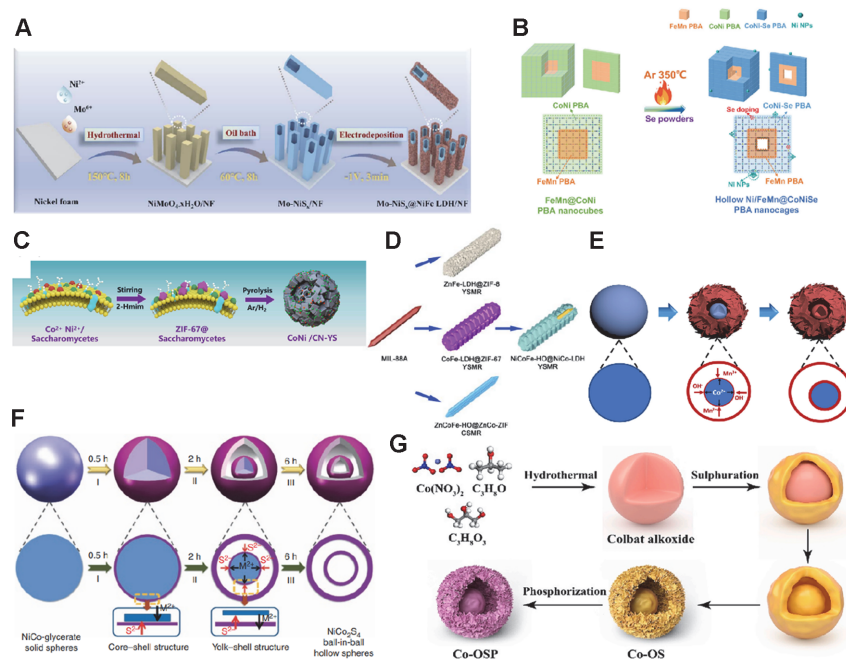
Fig. 5 Schematic illustration of the formation process of hollow core-shelled Mo-NiS$_x$@NiFe LDH/NF electrodes (A), synthesis diagram of hollow core-shelled PBA-Se-350 nanocages (B), synthesis diagram of hollow core-shelled CoNi/NC-YS (C), schematic illustration of hollow core-shelled NiCoFe-HO@NiCo-LDH YSMRs and related samples (D), synthesis diagram of hollow core-shelled Mn-CoP sphere (E), schematic illustration for the preparation of hollow double-shelled spheres NiCo$_2$S$_4$ (F) and synthesis diagram of hollow double-shelled Co-OSP-0.2 (G)

(A) Reprinted with permission from ref. [68], Copyright 2022, The Royal Society of Chemistry; (B) reprinted with permission from ref. [75], Copyright 2023, Wiley-VCH; (C) reprinted with permission from ref. [76], Copyright 2022, Elsevier; (D) reprinted with permission from ref. [78], Copyright 2022, Wiley-VCH; (E) reprinted with permission from ref. [79], Copyright 2021, Elsevier; (F) reprinted with permission from ref. [80], Copyright 2015, Nature; (G) reprinted with permission from ref. [81], Copyright 2023, Elsevier.
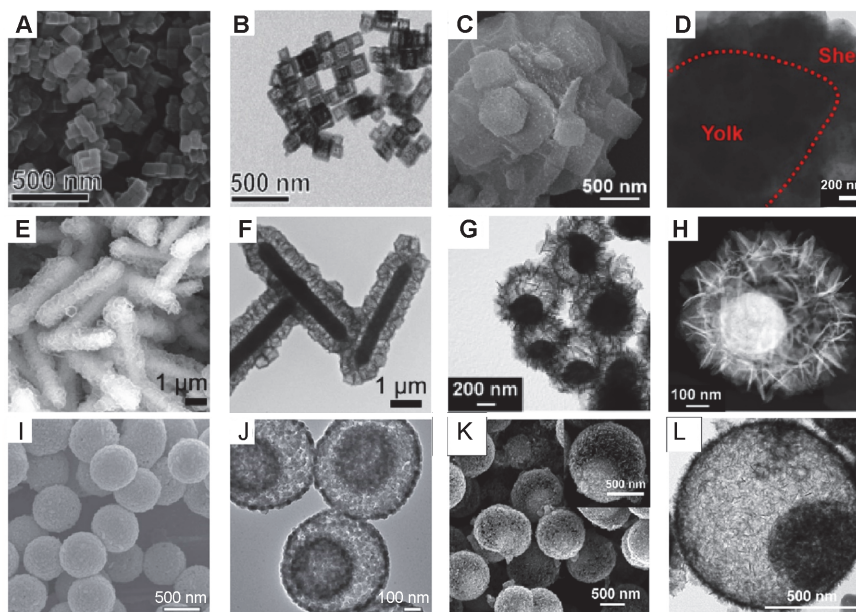
Fig. 6 SEM and TEM micrographs of hollow core-shelled PBA-Se-350 nanocages (A, B), SEM image and TEM image of hollow core-shelled CoNi/NC-YS (C, D), FESEM and TEM micrographs of hollow core-shelled NiCoFe-HO@NiCo-LDH YSMRs (E, F), TEM image and high-angle annular dark field TEM (HAADF-TEM) image for hollow core-shelled Mn-Co-P catalyst (G, H), FESEM image and TEM image of hollow double-shelled NiCo$_2$S$_4$ material (I, J) and SEM image and TEM image of hollow double-shelled Co-OSP-0.2 sphere (K, L)

(A, B) Reprinted with permission from ref. [75], Copyright 2023, Wiley-VCH; (C, D) reprinted with permission from ref. [76], Copyright 2022, Elsevier; (E, F) reprinted with permission from ref. [78], Copyright 2022, Wiley-VCH; (G, H) reprinted with permission from ref. [79], Copyright 2021, Elsevier; (I, J) reprinted with permission from ref. [80], Copyright 2015, Nature; (K, L) reprinted with permission from ref. [81], Copyright 2023, Elsevier.
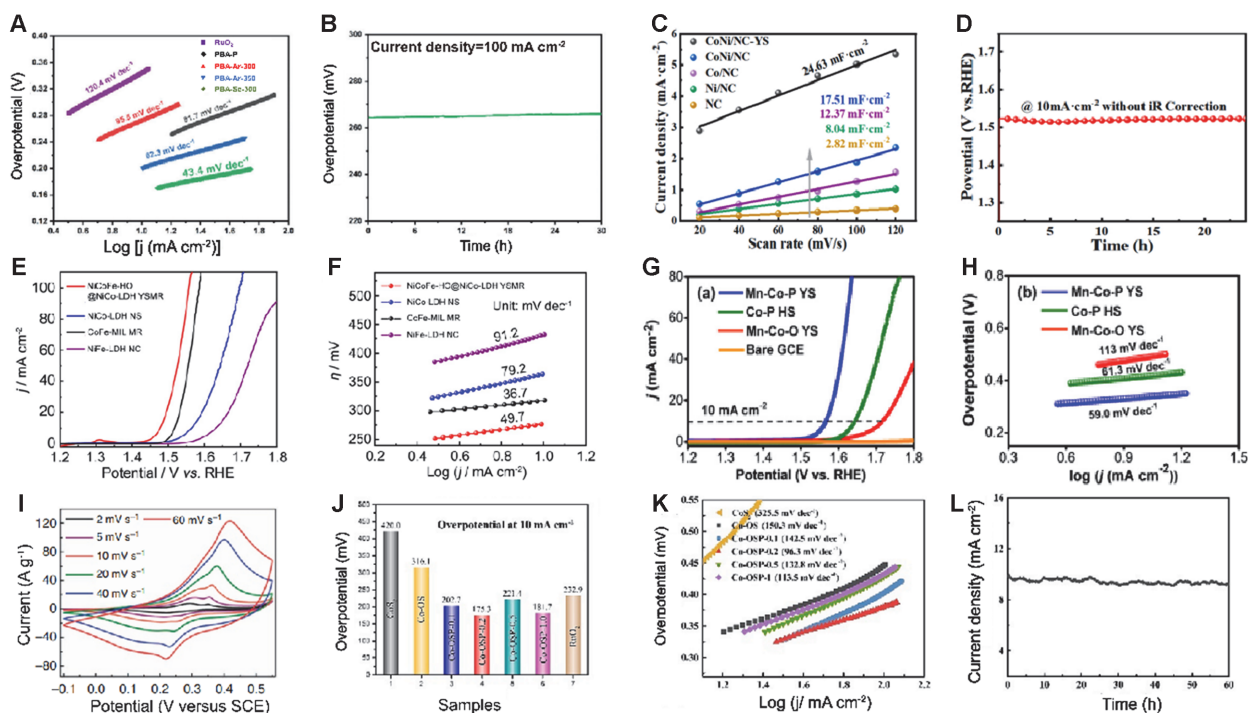
Fig. 7 Tafel slopes of hollow core-shelled PBA-Se 350 and other samples for OER (A), the chronopotentiometry measurement tested at 100 mA/cm² of PBA-Se-350 (B), the double-layer capacitances at different scan rates for hollow core-shelled CoNi/NC-YS (C), corresponding stability test at 10 mA/cm² (D), polarization curves of hollow core-shelled NiCoFe-HO@NiCo-LDH YSMRs and other materials (E), corresponding Tafel plots (F), LSV cures of hollow core-shelled Mn-Co-P (G), corresponding Tafel plots (H), cyclic voltammetry curves of hollow double shelled NiCo₂S₄ (I), overpotential at 10 mA/cm² for double shelled Co-OSP-0.2 sphere and other samples (J) and corresponding Tafel plots (K) and stability test at potential 1.48 V (L)

(A, B) Reprinted with permission from ref. [75], Copyright 2023, Wiley-VCH; (C, D) reprinted with permission from ref. [76], Copyright 2022, Elsevier; (E, F) reprinted with permission from ref. [78], Copyright 2022, Wiley-VCH; (G, H) reprinted with permission from ref. [79], Copyright 2021, Elsevier; (I) reprinted with permission from ref. [80], Copyright 2015, Nature; (J—L) reprinted with permission from ref. [81], Copyright 2023, Elsevier.

2.3 Ni/Co-based Hollow Double-shelled Structure Materials

Different from the hollow core-shelled structure, the inner structure of the hollow double-shelled structure is a hollow single-shelled material, which is similar to one bigger hollow structure hitched together with a smaller one, there is much free space between the inner and outer shells. Compared to hollow single-shelled and core-shelled structures, obviously, the hollow double-shelled structure can provide a larger void volume, a more effective electrocatalytic active surface area and a shorter ion-diffusion path, which has aroused extensive research.[82—84] Wherein, the mass diffusion/transfer and gas release kinetics can be accelerated, which enhances the catalytic performance and stability of Ni/Co-based electrocatalysts in water splitting.

A novel ternary nickel cobalt sulfide (NiCo₂S₄) hollow double-shelled structure has been developed *via* a facile solvothermal method by taking the uniform NiCo-glycerate spheres as the precursor with a subsequent sulfidation process. Wherein, the hollow core-shelled and double-

shelled structures are regulated by changing the reaction temperature during the anion exchange process (Fig. 5F).[80] The FESEM image and TEM images demonstrate that unique hollow double-shelled spheres with a roughness surface and more visible pores on the shell are observed (Fig. 6, I and J). In the cyclic voltammetry (CV) curves, two pairs of redox peaks are detected, indicating hollow double-shelled NiCo₂S₄ catalyst has redox reactions during the electrochemical test process. It may be due to the increased valency of the Ni²⁺ and Co²⁺ metal ions, which is conducive to the rapid redox reaction for NiCo₂S₄ hollow double-shelled spheres catalyst (Fig. 7I). Chong *et al.*[81] also reported a hierarchical nanosheets stacked Co-OSP-0.2 hollow double-shelled spheres electrocatalyst using a facile solvothermal method with the following sulfidation and subsequent phosphating process (Fig. 5G). The SEM image shows the spherical structure stacked by nanosheets of the Co-OSP-0.2 catalyst. The TEM image further reveals regular hollow double-shelled spheres with selenodont cavity (Fig. 6, K and L). The unique structure contributes to more accessible active sites, meanwhile promotes mass diffusion

kinetics. Thus, the hollow double-shelled spheres Co-OSP-0.2 electrocatalyst displays lower overpotential (175.3 mV) and smaller Tafel slope (96.3 mV/dec) than other catalysts, demonstrating fast reaction kinetics and excellent OER activity in 1 mol/L KOH (Fig. 7, J and K). Besides, the hollow double-shelled spheres Co-OSP-0.2 electrocatalyst displays long-time stability at the potential of 1.48 V for 60 h in an alkaline solution, meaning excellent activity and good stability, which benefits from the unique hollow double-shelled morphology with a large active surface area to produce accessible active sites (Fig. 7L).

Combining with the unique hollow double-shelled structure to construct heterojunction is an important strategy to enhance electrocatalytic activity. Kim $et.$ $al.$[85] have synthesized hollow double-shelled $NiSe_2$-FeSe polyhedrons (DHPs) via a self-supporting sacrificial template method following the etching, coprecipitation and selenization process (Fig. 8A). During the etching process, the MIL-88A polyhedrons were gradually etched by $CO(NH_2)_2$ and $Ni(NO_3)_2·6H_2O$, and the Fe species released and coprecipitated with Ni^{2+} and OH^- ions to form NiFe-LDH DHPs. The TEM images show that $NiSe_2$-FeSe DHPs are composed of hollow double-shelled polyhedron structure, and the inner shell is thicker than the outer shell (Fig. 9, A and B). The electrocatalytic activity is tested by the linear sweep voltammetry (LSV) measurement. The results show that the $NiSe_2$-FeSe DHPs display a lower overpotential of 280 mV and a smaller Tafel slope of 58 mV/dec at the current density of 10 mA/cm^2 than those of corresponding samples, demonstrating faster reaction kinetics and accelerating mass diffusion due to its unique porous double-shelled structure (Fig. 10, A and B). Accompanying the unique hollow double-shelled structure to dope metal ions is an effective approach to improving electrocatalytic activity as well. Wang et $al.$[11] have synthesized hollow double-shelled Cu-doped CoP NPs (DH-CuCo-P) coated on a carbon cloth (Fig. 8B). The structure of metal phosphide wrapped in carbon nanosheets can be adjusted from solid to hollow single-shelled, then to hollow double-shelled structure by controlling the composition of metal elements and the calcination conditions. Wherein, the Cu doping is the key to the formation of hollow double-shelled nanostructures, which is resulted from the Kirkendall effect. As depicted in SEM and TEM images, the carbon nanosheets are uniformly loaded with hollow double-shelled Cu-doped CoP NPs (Fig. 9, C and D). Interestingly, the hollow double-shelled DH-CuCo-P@NC/CC performs excellent HER activity with a smaller Tafel slope of 34.2 mV/dec in 1.0 mol/L KOH than hollow single-shelled and solid counterparts, benefiting from the unique hollow double-shelled structure for fast mass diffusion and fast reaction dynamics (Fig. 10, C and D).

2.4 Ni/Co-based HoMS Materials

The HoMS owns a shell upon shell structure, there is much free space between shells, which is similar to the multiple hollow single-shelled structure with different size nests to gather from smaller one to the bigger one, and many pores on the surface of the shell are achieved. We can call it "nano Chinese puzzle ball". Compared with the structures above mentioned as hollow single-shelled, hollow core-shelled or hollow double-shelled structures, obviously the HoMS has a higher specific surface area and better utilization of the inner space. It is conducive to accelerate superior electrochemical performance and good stability, benefiting from the special electronic structure engineering and unique HoMS hierarchical design. HoMS has great potential in lithium-ion batteries,[26,86−93] solar cells,[94−98] supercapacitors,[99] drug delivery[100−102] and electrocatalysis.[103−105] Wang's research group[106] has been devoted to the research of designing HoMS for many years, and has first proposed the sequential template method to synthesize various forms and compositions of HoMS. For example, hollow duplicated shells CoP catalyst (D-CoP-HoMSs) was constructed by a HoMSs Co_3O_4 sequential template method and subsequently phosphating process (Fig. 8C).[106] Because the Co atoms in Co_3O_4 diffuse outwards and the P atoms diffuse inwards slowly during the phosphating process, cavities form inside of the shell, which gather to form bubbles, and these bubbles fuse together again to form new shells. Ganesan et $al.$[107] have manufactured hollow multi-shelled CoS_2-MoS_2 spheres (CoS_2-MoS_2 HoMS) via solvothermal anion exchange and calcination process of Co-Schiff base (Fig. 8D). The SEM and TEM images show that the HoMS with a rough shell surface composed of nanoscale Co_3O_4 particles successfully is constructed after calcination (Fig. 9, E and F), which results in excellent performance. As shown in LSV curves, CoS_2-MoS_2 HoMS has a lower initial overpotential and a higher current density than other samples at the same scan rate. In addition, CoS_2-MoS_2 HoMS displays a slower Tafel slope (44.2 mV/dec) than IrO_2, indicating faster reaction kinetic due to the synergistic effect of CoS_2/MoS_2 heterojunction and unique HoMS (Fig. 10, E and F). Peng et $al.$[108] have synthesized a kind of spinel transitional metal oxides with a unique necklace-like HoMS by carbon template-assisted method. The HoMS is achieved by absorbing metal ions into necklace-like carbonaceous spheres as a template and proceeding a calcination process. Due to the rich oxygen vacancy by using the reduction of $NaBH_4$ solution in the multi-shelled NCO (R-NCO) catalysts, the excellent HER/OER activity and remarkable stability are demonstrated (Fig. 8E). As observed in SEM and TEM

images, a necklace-like HoMS is successfully synthesized (Fig. 9, G and H). Because of the unique necklace-like HoMS nanostructure to improve the reaction kinetics, a necklace-like R-NCO HoMS shows the smallest Tafel slope (45 mV/dec) for HER and the smallest Tafel slope (50 mV/dec) for OER than others, indicating that R-NCO HoMS can accelerate electron transfer and increase the reaction kinetics (Fig. 10, G and H).

Among various material architectures, HoMS exhibits several advantages, such as offering large effective electrocatalytic surface area and reducing diffusion lengths for mass transport.[109,110] Because of their high electrical conductivity and inherently adjustable electronic structure, transition metal phosphorus with HoMS structure has been studied extensively. For example, Zhang *et al*.[111] successfully have prepared a unique hollow triple-shelled microsphere CoP@CoP@(Co/Ni)₂P with a rich defect by using Co-BTC microspheres as a template (Fig. 8F). The SEM image exhibits a flower-like Co-BTC@Ni-LDH core-shelled structure that nanosheets attached to the spherical surface, which is attributed to the NiFe LDH-coating process. An obvious hollow triple-shelled structure can be seen by the TEM image after calcinations due to the non-uniform

shrinkage of LDH shell and Co-BTC core during the calcination process at high temperature (Fig. 9, I and J). And after a phosphating process, the unique CoP@CoP@(Co/Ni)₂P hollow triple-shelled microsphere is achieved. Furthermore, the HER activity of the catalyst is evaluated by electrochemical tests. The CoP@CoP@(Co/Ni)₂P hollow triple-shelled microsphere displays a smaller Tafel slope than commercial Pt/C, indicating its faster reaction kinetics. Besides, after 2000 cycles *via* a CV measurement, the polarization curve almost overlaps with the initial curve, which can be attributed to the synergistic effect of HoMS for a large number of active sites and rich defects at the interface of heterojunction for the enhanced intrinsic activity (Fig. 10, I and J).[111] Wang and co-worker[112] have designed a kind of HoMS CoNiP-0.25 catalyst by using MOF as self-sacrifice template and subsequently a phosphating process. Through SEM image, it can be seen that the HoMS CoNiP-0.25 catalyst can still maintain a spherical structure, and the HoMS with a rough surface can be clearly observed *via* the broken hollow sphere. The TEM image further demonstrates that the HoMS CoNiP-0.25 catalyst is a uniform layer-by-layer hollow spherical structure (Fig. 9, K and L). Furthermore, the HoMS CoNiP-0.25 catalyst displays
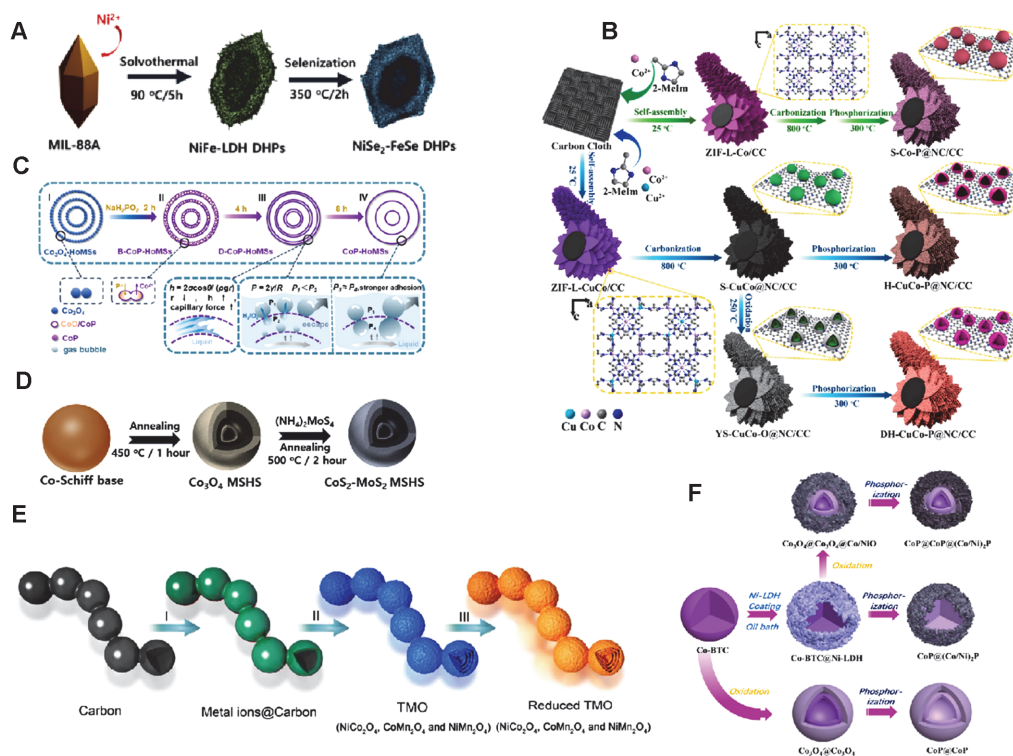
Fig. 8 Schematic illustration for the preparation of hollow double-shelled NiSe₂-FeSe DHPs (A), illustrated fabrication method and morphology evolution of S-Co-P@NC/CC, H-CuCo-P@NC/CC, and DH-CuCo-P@NC/CC composites with different embedded nanoparticles (B), schematic illustration of the forming process of D-CoP-HoMSs with different micro-nano structures of shell (C), schematic representation of the CoS₂-MoS₂ HoMSs (D), synthesis diagram of a necklace-like R-NCO HoMS (E) and the strategy of synthesizing hollow triple-shelled microsphere CoP@CoP@(Co/Ni)₂P and other samples (F)

(A) Reprinted with permission from ref. [85], Copyright 2021, American Chemical Society; (B) reprinted with permission from ref. [11], Copyright 2023, Elsevier; (C) reprinted with permission from ref. [106], Copyright 2021, Wiley-VCH; (D) reprinted with permission from ref. [107], Copyright 2020, Elsevier; (E) reprinted with permission from ref. [108], Copyright 2018, American Chemical Society; (F) reprinted with permission from ref. [111], Copyright 2023, Elsevier.
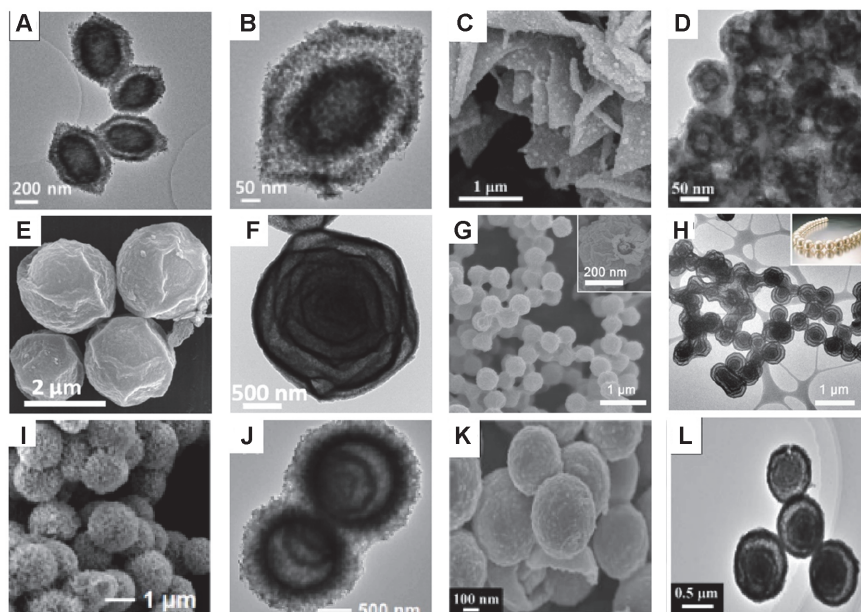
Fig. 9 TEM images of hollow double-shelled NiSe₂-FeSe DHPs (A, B), SEM and TEM images of DH-CuCo-P@NC/CC (C, D), SEM and TEM images of hollow double-shelled CoS₂-MoS₂ HoMS (E, F), SEM and TEM images of necklace-like R-NCO HoMS (G, H), SEM and TEM images of hollow triple-shelled CoP@CoP@(Co/Ni)₂P (I, J), SEM and TEM images of HoMS CoNiP-0.25 microspheres (K, L)

(A, B) Reprinted with permission from ref. [85], Copyright 2021, American Chemical Society; (C, D) reprinted with permission from ref. [11], Copyright 2023, Elsevier; (E, F) reprinted with permission from ref. [107], Copyright 2020, Elsevier; (G, H) reprinted with permission from ref. [108], Copyright 2018, American Chemical Society; (I, J) reprinted with permission from ref. [111], Copyright 2023, Elsevier; (K, L) reprinted with permission from ref. [112], Copyright 2019, The Royal Society of Chemistry.
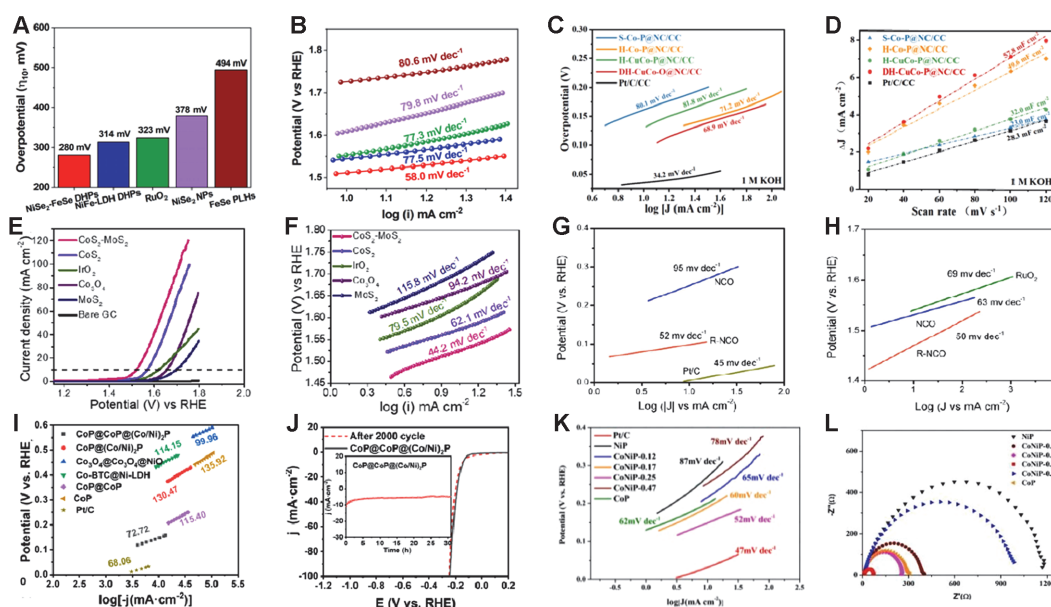
Fig. 10 Overpotential at a current density of 10 mA/cm² for hollow double-shelled NiSe₂-FeSe DHPs and different catalysts (A), corresponding Tafel plots (B), Tafel slopes for hollow double-shelled DH-CuCo-P@NC/CC and other catalysts for HER in 1 mol/L KOH (C), corresponding double-layer capacitances at different scan rates for DH-CuCo-P@NC/CC (D), LSV cures of CoS₂-MoS₂ HoMS and other catalysts (E), corresponding Tafel plots (F), Tafel plots of R-NCO HoMS for OER and HER (G, H), Tafel plots for hollow triple-shelled CoP@CoP@(Co/Ni)₂P and other materials for HER (I), polarization curves of the CoP@CoP@(Co/Ni)₂P microspheres before and after 2000 cycles (inset is stability test) (J), Tafel plots of HoMS CoNiP-0.25 microsphere and other catalysts (K), and corresponding Nyquist plots (L)

(A, B) Reprinted with permission from ref. [85], Copyright 2021, American Chemical Society; (C, D) reprinted with permission from ref. [11], Copyright 2023, Elsevier; (E, F) reprinted with permission from ref. [107], Copyright 2020, Elsevier; (G, H) reprinted with permission from ref. [108], Copyright 2018, American Chemical Society; (I, J) reprinted with permission from ref. [111], Copyright 2023, Elsevier; (K, L) reprinted with permission from ref.[112], Copyright 2019, The Royal Society of Chemistry.

outstanding HER activity due to the unique HoMS. As a result, the hollow multi-shelled CoNiP-0.25 catalyst possesses smaller resistance than others phosphating different ratios of Co/Ni in 1.0 mol/L KOH, indicating its excellent activity and good conductivity. In addition, the Tafel slope of hollow multi-shelled CoNiP-0.25 catalyst is comparable to that of commercial Pt/C for HER, which is favorable to the improvement of reaction kinetic (Fig. 10, K and L).[112]

In short, the unique multi-shelled hollow structure provides more active sites, which boosts the stability and

HER/OER activity of the electrocatalyst. Benefitting from large surface area, reduced diffusion charge transport, abundance of internal voids, and multiphase heterogeneous interfaces, HoMS has great application prospects in water splitting for HER/OER as shown in Table.1. However, the synthesis of HoMS is still challenging owing to the complexity of the structures. It is very crucial to comprehend the chemical reaction mechanism of HoMS during the preparation process by sequential templating approach, which is helpful to design ideal structures for various fields.

Table 1 HER/OER performances of overviewed hollow electrocatalysts.

Morphology	Material	Activity	Overpotential/mV	Current density/(mA·cm^{-2})	Tafel slope/(mV·dec^{-1})
Single-shelled hollow sphere	Co_3O_4/$CoMoO_4$-0.1-FO	OER	217	10	72
Single-shelled hollow nanocube	CoCu@HNC	HER	130	10	91.2
Single-shelled hollow sphere	CoFe/N-HCSs	OER	292	10	58
Double-shelled polyhedrons polyhedron	$NiSe_2$-FeSe DHPs	OER	280	10	58
Double-shelled carbon array	DH-CuCo-P@NC/CC	OER	177	10	84.1
Double-shelled carbon array	DH-CuCo-P@NC/CC	HER	85	10	68.9
Core-shelled carbon cage	CoNi/NC-YS	OER	292	10	53.8
Core-shelled hollow rod	NiS_x@NiFe LDH/NF	OER	224	10	44.41
Cored-shelled hollow rod	NiS_x@NiFe LDH/NF	HER	61.3	10	42.3
Multi-shelled sphere	D-CoP-HoMSs	OER	294	10	67
Multi-shelled sphere	D-CoP-HoMSs	HER	93	10	50
Multi-shelled necklace	RNCO	OER	240	10	50

3 Conclusion and Perspectives

Since electrochemical water splitting to produce hydrogen is a promising future fuel pathway, it has been essential that we seek bifunctional catalysts (HER/OER catalysts) with efficient, low cost and stable 0D Ni/Co-based hollow structure materials. As all we know, benefiting from large surface area, tunable shell architecture, and inner void space for reduced mass/charge transfer path, hollow structured electrocatalysts have been extensively studied, which provide an opportunity for the design of excellent electrocatalytic activity bifunctional catalysts. The 0D hollow Ni/Co-based hollow electrocatalysts from hollow single-shelled, core-shelled, double-shelled, then to HoMS are summarized. The recent progress in structure regulation and composition regulation of hollow Ni/Co-based electrocatalysts with different structures is reviewed. With the transformation of structure from single-shelled to multi-shelled, the relative contacting area between hollow particles is decreased due to the increased high utilization of internal

volume for high-performance electrocatalysts. Although great achievements have been achieved, there are challenges and shortcomings for the hollow Ni/Co-based HoMS electrocatalysts in the water splitting to produce hydrogen. First of all, we need to develop a simple process to simplify the synthesis process, as well as low-cost preparation synthesis methods to prepare efficient activity and durability hollow HoMS catalysts. Due to the complexity of synthesis steps, the scarcity of templates and the complexity of equipment in most synthesis methods, the research is greatly limited. Secondly, the mechanism of electrocatalysts with hollow HoMS structures in electrochemical water splitting still needs further study. Besides, the main barrier of HER and OER reactions is the slow reaction kinetics, simply designing hollow HoMS structure catalysts to enhance charge transport and increase surface active sites cannot decrease the reaction transition state. Finally, experimental instrumentation and characterization techniques as well as theoretical calculations need to be further deepened to reveal the true catalytic activity of species.

Acknowledgements

Conflicts of Interest

The authors declare no conflicts of interest.

References

[1] Zhang G. W., Li Z. Y., Zeng J. R., Yu L., Zuo C. Y., Wen P., Liu Y., Zhong L. B., Chen H. T., Qiu Y. J., *Appl. Catal. B: Environ.*, **2022**, *319*, 121921.

[2] Li R. W., Chen X. Y., Cao B. L., Ji R.Y., Deng Q. H., Qu J., Wang K. G., Zhu X. B., Chao Y., *Chem. Eng. J.*, **2021**, *409*, 128240.

[3] Li P., Li W. Q., Huang Y. Q., Huang Q. H., Tian S., *Small*, **2023**, *19*, 2300725.

[4] Li J. C., Zhang C., Zhang C., Ma H. J., Guo Z. Q., Zhong C. L., Xu M., Wang X. J., Wang Y. Y., Ma H. X., Qiu J. S., *Adv. Mater.*, **2022**, *34*, 2203900.

[5] Peng X., Xie S., Wang X., Pi C. R., Liu Z. T., Gao B., Hu L. S., Xiao W., Chu P. K., *J. Mater. Chem. A*, **2022**, *10*, 20761.

[6] Wang P., Luo Y. Z., Zhang G. X., Chen Z. S., Ranganathan H., Sun S. H., Shi Z. C., *Nano-Micro. Lett.*, **2022**, *14*, 120.

[7] Chen J. W., Chen H. X., Yu T. W., Li R. C., Wang Y., Shao Z. P., Song S. Q., *Electrochem. Energy Rev.*, **2021**, *4*, 566.

[8] Zhou Z., Pei Z. X., Wei L., Zhao S. L., Jian X., Chen Y., *Energy Environ. Sci.*, **2020**, *10*, 3185.

[9] Zhou Q. X., Xu C. X., Hou J. G., Ma W. Q., Jian T. Z., Yan S. S., Liu H., *Nano-Micro Lett.*, **2023**, *15*, 95.

[10] Liu Y., Xu S. J., Zheng X. Y., Lu Y. K., Li D., Jiang D. L., *Colloid Interface Sci.*, **2022**, *625*, 457.

[11] Wang X., Huang H. G., Qian J. J., Li Y. W., Shen K., *Appl. Catal. B: Environ.*, **2023**, *325*, 122295.

[12] Jiang S., Xiao T. Y., Xu C., Wang S. W., Peng H. Q., Zhang W. J., Liu B., Song Y. F., *Small*, **2023**, *19*, 2208027.

[13] Chen J. W., Chen H. X., Yu T. W., Li R. C., Wang Y., Shao Z. P., Song S. Q., *Electrochem. Energy Rev.*, **2021**, *4*, 566.

[14] Zhang Z., Ma X. X., Tang J. L., *J. Mater. Chem. A*, **2018**, *6*, 12361.

[15] Wu D. L., Liu B., Li R. D., Chen D., Zeng W. H., Zhao H. Y., Yao Y. T., Qin R., Yu J., Chen L., Zhang J. N., Li B., Mu S. C., *Small*, **2023**, *19*, 2300030.

[16] Jian J., Yuan L., Li H., Liu H. H., Zhang X. H., Sun X. J., Yuan H. M., Feng S. H., *Chem. Res. Chinese Universities*, **2019**, *35*, 179.

[17] Chen P. Z., Feng D. M., Li K. X., Tong Y., *Dalton Trans.*, **2022**, *51*, 16990.

[18] You B., Tang M. T., Tsai C., Abild-Pedersen F., Zheng X. L., Li H., *Adv. Mater.*, **2019**, *31*, 1807001.

[19] Wang J., Tran D. T., Chang K., Prabhakaran S., Kim D. H., Kim N. H., Lee J. H., *Energy Environ. Mater.*, **2022**, *6*, e12526.

[20] Ahasan Habib M., Mandavkar R., Lin S., Burse S., Khalid T., Hasan Joni. M., Jeong J. H., Lee J., *Chem. Eng. J.*, **2023**, *462*, 142177.

[21] Zhao T. W., Wang Y., Karuturi S., Catchpole K., Zhang Q., Zhao C., *Carbon Energy*, **2020**, *2*, 582.

[22] Zhang W. Y., Chao Y. G., Zhang W. S., Zhou J. H., Lv F., Wang K., Lin F. X., Luo H., Li J., Tong M. P., *Adv. Mater.*, **2021**, *33*, 2102576.

[23] Baek J., Hossain M. D., Mukherjee P., Lee J., Winther K. T., Leem J., Jiang Y., Chueh W. C., Bajdich M., Zheng X., *Nat. Commun.*, **2023**, *14*, 5936.

[24] Chen R. Z., Chen S. H., Wu W., Zhu Y., Zhong J., Cheng N. C., *ACS Energy Lett.*, **2023**, *8*, 3504.

[25] Yang X., Cheng J., Li H., Xu Y., Tu W. F., Zhou J. H., *Chem. Eng. J.*, **2023**, *465*, 142745.

[26] Wang C. R., Zhang L., Dou Y. H., Hencz L., Jiang L. X., AlMamun M., Liu P. R., Zhang S. Q., Wang D., Zhao H. J., *Energy Technol.*, **2020**, *8*, 2000008.

[27] Jeon S. S., Kang P. W., Klingenhof M., Lee H., Dionigi F., Strasser P., *ACS Catal.*, **2023**, *13*, 1186.

[28] Ni Y. M., Shi D., Mao B. G., Wang S. H., Wang Y., Ahmad A., Sun J. L., Song F., Cao M. H., Hu C. W., *Small*, **2023**, *19*, 2302556.

[29] Chanda D., Kwon H., Meshesha M. M., Gwon J. S., Ju M., Kim K., Yang B. L., *Appl. Catal. B: Environ.*, **2024**, *340*, 123187.

[30] Li X., Kou Z. K., Xi S. B., Zang W. J., Yang T., Zhang L., Wang J. H., *Nano Energy*, **2020**, *78*, 105230.

[31] Huang W. H., Li X. M., Yang X. F., Zhang H. Y., Liu P. B., Ma Y. M., Lu X., *Chem. Eng. J.*, **2021**, *420*, 127595.

[32] Zhang L., Rong J., Yang Y., Zhu H., Yu X., Chen C., Cheng H. M., Liu G., *Small*, **2023**, *19*, 2207472.

[33] Lyu C., Cheng J. R., Wang H. C., Yang Y. Q., Wu K. L., Song P., Lau W. M., Zheng J. L., Zhu X. X., Yang H. Y., *Adv. Compos. Hybrid Mater.*, **2023**, *6*, 175.

[34] Xu D. X., Liu S. R., Zhang M. Y., Xu L. L., Gao H., Yao J., *Small*, **2023**, *19*, 2300201.

[35] Xie X. Q., Liu J., Gu C., Li J., Zhao Y., Liu C. S., *J. Energy Chem.*, **2022**, *64*, 503.

[36] Jia H. Y., Wang H. Y., Yan F. F., Zhang H. C., Li Z., Wang J. J., *Appl. Catal. B: Environ.*, **2023**, *343*, 123362.

[37] Gao X. R., Liu X. M., Zang W. J., Dong H. L., Pang Y. J., Kou Z. K., Wang P. Y., Pan Z. H., Wei S. R., Mu S. C., Wang J. H., *Nano Energy*, **2020**, *78*, 105355.

[38] Zhang K. K., Mai W. S., Li J., Li G. Q., Tian L. H., Hu W., *ACS Appl. Nano Mater.*, **2019**, *2*, 5931.

[39] Li P., Qiang F. F., Tan X. H., Li Z., Shi J., Liu S., Huang M. H., Chen J. W., Tian W. Q., Wu J. Y., Hu W., Wang H. L., *Appl. Catal. B: Environ.*, **2024**, *340*, 123231.

[40] Zhang Z. J., Guo J. P., Sun S. H., Sun Q., Zhao Y. W., Zhang Y. F., Yu Z. Y., Li C. S., Sun Y., Zhang M. M., Jiang Y., *Rare Met.*, **2023**, *42*, 3607.

[41] Liu Q., Li M. Y., Shi Y. M., Liu C. B., Yu Y. F., Zhang B., *Rare Met.*, **2021**, *41*, 836.

[42] Chen M. X., Li H. J., Wu C. L., Liang Y. B., Qi J., Li J., Shangguan E., Zhang W., Cao R., *Adv. Funct. Mater.*, **2022**, *32*, 2206407.

[43] Qi Y. X., Li T. T., Hu Y. J., Xiang J. H., Shao W. Q., Chen W. H., Mu X. Q., Liu S. L., Chen C. Y., Yu M., Mu S. C., *Chem. Res. Chinese Universities*, **2022**, *38*, 1282.

[44] Yang M., Zhang C. H., Li N. W., Luan D., Yu L., Lou X. W., *Adv. Sci.*, **2022**, *9*, 2105135.

[45] Qi X. R., Liu Y., Ma L. L., Hou B. X., Zhang H. W., Li X. H., Wang Y. S., Hui Y. Q., Wang R. X., Bai C.Y., Liu H., Song J. J., Zhao X. X., *Rare Met.*, **2022**, *41*, 1637.

[46] Zhao X. X., Wang J. Y., Yu R. B., Wang D., *J. Am. Chem. Soc.*, **2018**, *140*, 17114.

[47] Zong L. B., Xu J., Jiang S. Y., Zhao K., Wang Z. M., Liu P. R., Zhao H. J., Chen J., Xing X. R., Yu R. B., *Adv. Mater.*, **2016**, *29*, 1604377.

[48] Ma L. L., Hou B. X., Zhang H., Yuan S. T., Zhao B., Liu Y., Qi X. R., Liu H. Y., Zhang S. H., Song J. J., Zhao X. X., *Chem. Eng. J.*, **2023**, *453*, 139735.

[49] Zhang H., Wang L., Ma L. L., Liu Y. H., Hou B. X., Shang N. Z., Zhang S. H., Song J. J., Chen S. Q., Zhao X. X., *Adv. Sci.*, **2023**, 2306168.

[50] Feng J. N., Shi C., Dong H. H., Zhang C. Y., Liu W. D., Liu Y., Wang T. Y., Zhao X. X., Chen S. Q., Song J. J., *J. Energy Chem.*, **2023**, *86*, 135.

[51] Liu J. C., Ma L. L., Li S., Hou L. L., Qi X. R., Wen Y. Q., Hu G. P., Wang N., Zhao Y., Zhao X. X., *Rare Met.*, **2023**, *42*, 3378.

[52] Ma L. L., Hou B. X., Shang N. Z., Zhang S. H., Wang C., Zong L. B., Song J. J., Wang J. Y., Zhao X. X., *Mater. Chem. Front.*, **2021**, *5*, 4579.

[53] Fan C., Wu X. D., Li M., Wang X., Zhu Y., Fu G. T., Ma T. Y., Tang Y. W., *Chem. Eng. J.*, **2022**, *431*, 133829.

[54] Ma L. L., Zhou X. M., Sun J., Zhang P., Hou B. X., Zhang S. H., Shang N. Z., Song J. J., Ye H. J., Shao H., Tang Y. F., Zhao X. X., *J. Energy Chem.*, **2023**, *82*, 268.

[55] Du J., Chen D. X., Ding Y. X., Wang L. Q., Li F., Sun L. C., *Small*, **2023**, *19*, 2207611.

[56] Wang C., Shang H. Y., Li J., Wang Y., Xu H., Wang C. Y., Guo J., Du Y. K., *Chem. Eng. J.*, **2021**, *420*, 129805.

[57] Zhang J., Hu L. P., Cao W., Dong Y. Y., Xia D. B., Lin K. F., Yang Y. L., *Inorg. Chem.*, **2023**, *62*, 11690.

[58] Wang W., Zhang J., Lin K. F., Wang J. Q., Hu B. Y., Dong Y. Y., Xia D. B., Yang Y. L., *J. Energy Chem.*, **2023**, *86*, 308.

[59] Yu L., Yang J. F., Guan B. Y., Lu Y., Lou X. W., *Angew. Chem. Int. Ed.*, **2017**, *57*, 172.

[60] Qian Q., Li Y. P., Liu Y., Zhang G. Q., *Appl. Catal. B*: *Environ.*, **2020**, *266*, 118642.

[61] Zhu Y. X., Zhang L., Zhang X., Li Z., Zha M., Li M., Hu G. Z., *Chem. Eng. J.*, **2021**, *405*, 127002.

[62] Xia L. C., Bo L. L., Shi W. P., Zhang Y. N., Shen Y. X., Ji X. C., Guan X. L., Wang Y. X., Tong J. H., *Chem. Eng. J.*, **2023**, *452*, 139250.

[63] Li J. M., Kang Y. M., Wei W. L., Li X., Lei Z. Q., Liu P., *Chem. Eng. J.*, **2021**, *407*, 127961.

[64] Guo Y. N., Zhou X., Tang J., Tanaka S., Kaneti Y. V., Na J., Jiang B., Yamauchi Y., Bando Y., Sugahara Y., *Nano Energy,* **2020**, *75*, 104913.

[65] Ding X. D., Pei L. S., Huang Y. X., Chen D. Y., Xie Z. L., *Small*, **2022**, *18*, 2205547.

[66] Zhang Z. Q., Zhang Z., Chen X. B., Wang H. B., Lu H. Y., Shi Z., Feng S. H., *CCS Chem.*, **2024**, *6*, 1324.

[67] Guo R. K., Shi W., Liu W. Z., Yang X., Xie Y., Yang T., Xiao J. F., *Chem. Eng. J.*, **2022**, *429*, 132478.

[68] Li Y. Y., Guo H. R., Zhang Y., Zhang H. T., Zhao J. Y., Song R., *J. Mater. Chem. A*, **2022**, *10*, 18989.

[69] Lu X. F., Zhang S. L., Sim W. L., Gao S. Y., Lou X. W., *Angew. Chem. Int. Ed.*, **2021**, *60*, 22885.

[70] Luo J. H., Wang J., Guo Y., Zhu J. W., Jin H. H., Zhang Z. W., Zhang D. J., Niu Y. S., Hou S. G., Du J. M., He D. P., Xiong Y. L., Chen L., Mu S. C., Huang Y., *Appl. Catal. B*: *Environ.*, **2022**, *305*, 121043.

[71] Liu Y., Lin Q., Chen X. C., Meng X. F., Hou B. X., Liu H. Y., Zhang S. H., Shang N. Z., Wang Z., Zhang C. Y., Song J. J., Zhao X. X., *Energy Environ. Mater.*, **2023**, e12684.

[72] Song W. J., Teng X., Niu Y. L., Gong S. Q., He X. M., Chen Z. F., *Chem. Eng. J.*, **2021**, *409*, 128227.

[73] Zhang K. F., Deng Y. Q., Wu Y. H., Wang L. L., Yan L. F., *J. Colloid Interface Sci.*, **2023**, *647*, 246.

[74] Wen J. G. L., Li Y. W., Gao J. K., *Chem. Res. Chinese Universities*, **2020**, *36*, 662.

[75] Wang S., Huo W., Feng H., Xie Z., Shang J. K., Formo E. V., Camargo P. H. C., Fang F., Jiang J., *Adv. Mater.*, **2023**, *35*, 2304494.

[76] Hou G. Y., Jia X., Kang H. J., Qiao X. S., Liu Y., Li Y., Wu X. H., Qin W., *Appl. Catal. B, Environ.*, **2022**, *315*, 121551.

[77] Hu L. Y., Xiao R. S., Wang X., Wang X. X., Wang C. L., Wen J., Gu W. L., Zhu C. Z., *Appl. Catal. B*: *Environ.*, **2021**, *298*, 120599.

[78] Niu Q., Yang M., Luan D., Li N. W., Yu L., Lou X. W., *Angew. Chem. Int. Ed.*, **2022**, *61*, e202213049.

[79] Kaneti Y. V., Guo Y., Septiani N. L. W., Iqbal M., Jiang X., Takei T., Yuliarto B., Alothman Z. A., Golberg D., Yamauchi Y., *Chem. Eng. J.*, **2021**, *405*, 126580.

[80] Shen L., Yu L., Wu H. B., Yu X. Y., Zhang X., Lou X. W., *Nat. Commun.*, **2015**, *6*, 6694.

[81] Chong B., Xia M. Y., Lv Y., Li H., Yan X. Q., Lin B., Yang G. D., *Chem. Eng. J.*, **2023**, *465*, 142853.

[82] Wei Y. Z., Zhao D. C., Wan J. W., Wang D., *Trends Chem.*, **2022**, *4*, 1021.

[83] Ding D. N., Shen K., Chen X. D., Chen H. R., Chen J. Y., Fan T., Wu R. F., Li Y. W., *ACS Catal.*, **2018**, *8*, 7879.

[84] Li G. D., Tang Z. Y., *Nanoscale*, **2014**, *6*, 3995.

[85] Ramesh S. K., Ganesan V., Kim J., *ACS Appl. Energy Mater.*, **2021**, *4*, 12998.

[86] Wang J. Y., Tang H. J., Wang H., Yu R. B., Wang D., *Mater. Chem. Front.*, **2017**, *1*, 414.

[87] Xu W., Bi R. Y., Yang M., Wang J. Y., Yu R. B., Wang D., *Nano Res.*, **2023**, *16*, 12745.

[88] Zhao J. L., Wang J. Y., Bi R., Yang. M., Wang J. W., Jiang H. Y., Gu L., Wang D., *Angew. Chem. Int. Ed.*, **2021**, *60*, 25719.

[89] Chang Z. H., Liu W. D., Feng J. N., Lin Z. H., Shi C., Wang T. Y., Lei Y. J., Zhao X. X., Song J. J., Wang G. X., *Batteries Supercaps*, **2023**, e202300516.

[90] Zhao X. L., Yang M., Wang J. Y., Wang D., *Chem. Res. Chinese Universities*, **2023**, *39*, 630.

[91] Wang J. Y., Yang N. L., Tang H. J., Dong Z. H., Jin Q., Yang M., Kisailus D., Zhao H. J., Tang Z. Y., Wang D., *Angew. Chem. Int. Ed.*, **2013**, *52*, 6417.

[92] Wang J. Y., Tang H. J., Zhang Y. J., Ren H., Yu R. B., Jin Q., Qi J., Mao D., Yang M., Wang Y., Liu P. R., Zhang Y., Wen Y. R., Gu L., Ma G. H., Su Z. G., Tang Z. Y., Zhao H. J., Wang D., *Nat. Energy*, **2016**, *1*, 16050.

[93] Zhao X. L., Yang M., Wang J. Y., Wang D., *Chem. Res. Chinese Universities*, **2023**, *39*, 630.

[94] Dong Z., Ren H., Hessel C. M., Wang J. Y., Yu R. B., Jin Q., Yang M., Hu Z. D., Chen Y. F., Tang Z. Y., Zhao H. J., Wang D., *Adv. Mater.*, **2013**, *26*, 905.

[95] Wei Y., Wang J., Yu R., Wan J., Wang D., *Angew. Chem. Int. Ed.*, **2019**, *58*, 1422.

[96] Wang W., Zhang J., Lin K. F., Wang J. Q., Zhang X. R., Hu B. Y., Dong Y. Y., Xia D. B., Yang Y. L., *Adv. Mater.*, **2023**, *35*, 2306140.

[97] Hu B. Y., Zhang J., Yang Y. L., Dong Y. Y., Wang J. W. Q., Wang W., Lin K. F., Xia D. B., Fan R. Q., *Nano Energy*, **2023**, *118*, 109022.

[98] Han W. S., Wang Y. L., Wan J. W., Wang D., *Chem. Res. Chinese Universities*, **2022**, *38*, 117.

[99] Wang C., Wang J. Y., Hu W. P., Wang D., *Chem. Res. Chinese Universities*, **2019**, *36*, 68.

[100] Zhao D. C., Wei Y. Z., Xiong J., Gao C. S., Wang D., *Adv. Funct. Mater.*, **2023**, *33*, 2300681.

[101] Zhao D. C., Yang N. L., Wei Y., Jin Q., Wang Y. L., He H. Y., Yang Y., Han B., Zhang S. J., Wang D., *Nat. Commun.*, **2020**, *11*, 4450.

[102] Yuan M. W., Shi S. L., Luo Y. P., Yu Y., Wang S. H., Chen C., *Chem. Res. Chinese Universities,* **2022**, *38*, 999.

[103] Wang L., Wan J. W., Zhao Y. S., Yang N. L., Wang D., *J. Am. Chem. Soc.*, **2019**, *141*, 2238.

[104] Wang H., Yang N. L., Cui W., Wang J. Y., Li Q. H., Zhang Q. H., Yu X. Q., Gu L., Li J., Yu R. B., Huang K. K., Song S. Y., Feng S. H., Wang D., *Angew. Chem. Int. Ed.*, **2020**, *59*, 19691.

[105] Wang H., Mao D., Qi J., Zhang Q. H., Ma X. H., Song S. Y., Gu L., Yu R. B., Wang D., *Adv. Funct. Mater.*, **2019**, *29*, 1806588.

[106] Hou P., Li D., Wan J. W., Zhang C. H., Zhang X. Q., Jiang H. Y., Zhang Q. H., Gu L., Wang D., *Angew. Chem. Int. Ed.*, **2021**, *60*, 6926.

[107] Ganesan V., Kim J., *Int. J. Hydrogen Energy*, **2020**, *45*, 13290.

[108] Peng S. J., Gong F., Li L. L., Yu D. S., Ji D. X., Zhang T., Hu Z., Zhang Z. Q., Chou S. L., Du Y. H., Ramakrishna S., *J. Am. Chem. Soc.*, **2018**, *140*, 13644.

[109] Li B., Wang J. Y., Bi R. Y., Yang N. L., Wan J. W., Jiang H. Y., Gu L., Du J., Cao A. M., Gao W., Wang D., *Adv. Mater.*, **2022**, *34*, 2200206.

[110] Huang T. Y., Yang M., Wang J. Y., Zhang S. J., Du J., Wang D., *Chem. J. Chinese Universities*, **2022**, *43*, 20220263.

[111] Zhang H., Wu Y. Q., Wang X. D., Li C. P., Xiao Z. Y., Liu Y. R., Deng Y., Li Z. J., Wang L., *Chem. Eng. J.*, **2023**, *463*, 142448.

[112] Du Y. M., Zhang M. J., Wang Z. C., Liu Y. R., Liu Y. J., Geng Y. L., Wang L., *J. Mater. Chem. A*, **2019**, *7*, 8602.

Chem. Res. Chinese Universities, 2024, 40(3), 437—450

450

https://doi.org/10.1007/s40242-024-3278-3